Sidestream Dark Field (SDF) imaging: a novel stroboscopic LED ring-based imaging modality for clinical assessment of the microcirculation.

P. T. Goedhart‡, M. Khalilzada‡, R. Bezemer‡, J. Merza, and C. Ince*

Department of Physiology, Academic Medical Center, University of Amsterdam, Meibergdreef 9, 1105 AZ Amsterdam, the Netherlands
‡These authors contributed equally to this work.
**Corresponding author: C.Ince@amc.uva.nl*

Abstract: Sidestream Dark Field (SDF) imaging, a stroboscopic LED ring-based imaging modality, is introduced for clinical observation of the microcirculation. SDF imaging is validated by comparison to Orthogonal Polarization Spectral imaging. Nailfold capillary diameters and red blood cell velocities were measured using both techniques and equal quantitative results were obtained. An image quality system was developed to quantitatively compare the quality of sublingually-acquired microcirculatory images using OPS and SDF imaging. Venular contrast, sharpness, and quality were shown to be comparable for OPS and SDF imaging. However, capillary contrast and quality were shown to be significantly higher using SDF imaging. Venular granularity, in addition, was more clearly observable using SDF imaging.

OCIS codes: (170.0110) Imaging systems; (110.0180) Microscopy; (170.5380) Physiology

References

1. B. Fagrell and A. Bollinger, eds., *Clinical Capillaroscopy* (Hogrefe & Huber, 1990).
2. B. Fagrell, A. Fronek, and M. Intaglietta, "A microscope-television system for studying flow velocity in human skin capillaries," Am. J. Physiol. Heart Circ. Physiol. **233**, 318-321 (1977).
3. D. W. Slaaf, G. J. Tangelder, R. S. Reneman, K. Jager, and A. Bollinger, "A versatile incident illuminator for intravital microscopy," Int. J. Microcirc. Clin. Exp. **6**, 391-397 (1987).
4. W. Groner, J. W. Winkelman, A. G. Harris, C. Ince, G. J. Bouma, K. Messmer, and R. G. Nadeau, "Orthogonal polarization spectral imaging: a new method for study of the microcirculation," Nat. Med. **5**, 1209-1212 (1999).
5. S. Trzeciak, R. P. Dellinger, J. E. Parrillo, M. Guglielmi, J. Bajaj, N. L. Abate, R. C. Arnold, S. Colilla, S. Zanotti, and S. M. Hollenberg, "Early microcirculatory perfusion derangements in patients with severe sepsis and septic shock: relationship to hemodynamics, oxygen transport, and survival," Ann. Emerg. Med. **49**, 88-98 (2007).
6. P. E. Spronk, C. Ince, M. J. Gardien, K. R. Mathura, H. M. Oudemans-van Straaten, and D. F. Zandstra, "Nitroglycerin in septic shock after intravascular volume resuscitation," Lancet **360**, 1395-1396 (2002).
7. Y. Sakr, M. J. Dubois, D. de Backer, J. Creteur, and J. L. Vincent, "Persistent microcirculatory alterations are associated with organ failure and death in patients with septic shock," Crit. Care Med. **32**, 1825-1831 (2004).
8. D. de Backer, J. Creteur, M. J. Dubois, Y. Sakr, and J. L. Vincent, "Microvascular alterations in patients with acute severe heart failure and cardiogenic shock," Am. Heart J. **147**, 91-99 (2004).
9. A. Dubin, E. V. S. Kanoore, M. Pozo, G. Murias, C. Canullán, E. Martins, G. Ferrara, H. Canales, M. Laporte, E. Estenssoro, and C. Ince, "Persistent villi hypoperfusion explains intramucosal acidosis in sheep endotoxemia," Crit. Care Med. (in press).
10. E. C. Boerma, P. H. J. van der Voort, P. E. Spronk, and C. Ince, "Relationship between sublingual and intestinal microcirculatory perfusion in patients with abdominal sepsis," Crit. Care Med. **35**, 1055-1060 (2007).

#86192 - $15.00 USD Received 7 Aug 2007; revised 11 Oct 2007; accepted 25 Oct 2007; published 31 Oct 2007

11. J. A. H. Lindeboom, K. R. Mathura, I. H. Aartman, F. Kroon, and C. Ince, "The influence of the application of platelet enriched plasmas in oral mucosal wound healing," Clin. Oral Impl. Res. **18**, 133-139 (2007).
12. A. M. Dondorp, C. Ince, P. Tipmanee, J. Hanson, A. van Kuijen, M. A. Faiz, M. R. Rahman, M. Hasan, E. Bin Yunus, A. Ghose, R. Ruangveerayut, D. Limmathurotsakul, K. R. Mathura, N. J. White, and N. P. J. Day, "Direct in-vivo assessment of microcirculatory dysfunction in severe falciparum malaria," J. Infect. Dis. (in press).
13. F. Pennings, G. J. Bouma, and C. Ince, "Direct observation of the human cerebral microcirculation during aneurysm surgery reveals increased arteriolar contractility," Stroke **35**, 1284-1288 (2004).
14. K. R. Mathura, G. J. Bouma, and C. Ince, "Abnormal microcirculation in brain tumors during surgery," Lancet **358**, 1698-1699 (2001).
15. C. Ince, "The microcirculation is the motor of sepsis," Crit. Care **9**, Suppl. 4, 13-19 (2005).
16. D. de Backer, J. Creteur, J. C. Preiser, M. J. Dubois, and J. L. Vincent, "Microvascular blood flow is altered in patients with sepsis," Am. J. Respir. Crit. Care Med. **166**, 98-104 (2002).
17. H. A. Lehr, F. Bittinger, and C. J. Kirkpatrick, "Microcirculatory dysfunction in sepsis: a pathogenetic basis for therapy?" J. Pathol. **190**, 373-386 (2000).
18. D. R. Dantzker, "Adequacy of tissue oxygenation," Crit. Care Med. **21**, Suppl. 2, 40-43 (1993).
19. J. Lindert, J. Werner, M. Redlin, H. Kuppe, H. Habazettl, and A. R. Pries, "OPS imaging of human microcirculation: a short technical report," J. Vasc. Res. **39**, 368-372 (2002).
20. V. Cerný, Z. Turek, and R. Pařízková, "Orthogonal Polarization Spectral imaging: a review," Physiol. Res. **56** (2007).
21. M. Heger, J. F. Beek, K. Stenback, D. J. Faber, and M. J.C. van Gemert, "Darkfield orthogonal polarized spectral imaging for studying endovascular laser-tissue interactions in vivo – a preliminary study," Opt. Express **13**, 702-715 (2005).
22. C. Ince, "Sidestream dark field imaging: an improved technique to observe sublingual microcirculation," Crit. Care **9**, Suppl. 1, 72 (2005).
23. Z. Turek, V. Cerný, and R. Pařízková, "Noninvasive in vivo assessment of the skeletal muscle and small intestine serous surface microcirculation in rat: sidestream dark-field (SDF) imaging," Physiol. Res. **56** (2007).
24. *Visible and near infrared absorption spectra of human and animal haemoglobin determination and application*, W. G. Zijlstra, A. Buursma, and O. W. van Assendelft, eds. (Brill Academic Publishers, 2000).
25. D. de Backer, S. Hollenberg, C. Boerma, P. T. Goedhart, G. Büchele, G. Ospina-Tascon, I. Dobbe, and C. Ince, "How to evaluate the microcirculation? Report of a round table conference," Crit. Care (in press).
26. K. R. Mathura, K. C. Vollebergt, K. Boer, J. C. de Graaf, D. T. Ubbink, and C. Ince, "Comparison of OPS imaging and conventional capillary microscopy to study the human microcirculation," J. Appl. Physiol. **91**, 74-78 (2001).
27. T. K. Bergersen, M. Eriksen, and L. Walloe, "Effect of local warming on hand and finger artery blood velocities," Am. J. Physiol. Regul. Integr. Comp. Physiol. **269**, 325-330 (1995).
28. J. M. Bland and D. G. Altman, "Statistical methods for assessing agreement between two methods of clinical measurement," Lancet **1**, 307-310 (1986).
29. J. M. Bland and D. G. Altman, "Comparing methods of measurement: why plotting difference against standard method is misleading," Lancet **346**, 1085-1087 (1995).
30. C. G. Ellis, M. L. Ellsworth, R. N. Pittman, and W. L. Burgess, "Application of image analysis for evaluation of red blood cell dynamics in capillaries," Microvasc. Res. **44**, 214-225 (1992).
31. J. G. G. Dobbe, G. J. Streekstra, B. Atasever, R. van Zijderveld, and C. Ince, "Measurement of functional microcirculatory geometry and velocity distributions using automated image analysis," submitted to Microcirculation.
32. K. R. Mathura, L. Alic, and C. Ince, "Initial clinical experience with OPS imaging for observation of the human microcirculation," in: *Yearbook of intensive care and emergency medicine*, J. L. Vincent, ed. (Springer, 2001).

1. Introduction

Up to one decade ago, direct intravital observation of the microcirculation in humans was limited to the use of bulky capillary microscopes, mainly applied to the nailfold capillary bed, thus severely limiting microcirculatory investigation under clinical conditions [1,2]. The introduction of Orthogonal Polarization Spectral (OPS) imaging by Slaaf et al. and its implementation into a clinically-applicable hand-held microscope opened the field of studying the human microcirculation in exposed organ and tissue surfaces [3,4]. Since then, numerous studies have been undertaken in various clinical scenarios where cardiovascular function is at risk. Studies have especially been made in investigating disease and therapy

#86192 - $15.00 USD Received 7 Aug 2007; revised 11 Oct 2007; accepted 25 Oct 2007; published 31 Oct 2007

during surgery, emergency medicine, and intensive care medicine [5-10] as well as during such diverse conditions as cancer, wound healing, and infectious diseases [11-14]. OPS imaging has had an important clinical impact by observation of the sublingual microcirculation during sepsis, shock, and resuscitation [6,7,15-17]. Results from several medical centers have shown that OPS observation of sublingual microcirculatory (perfusion) alterations provided more sensitive information about patient outcome from sepsis and shock than conventional clinical parameters do. These microcirculatory alterations have been shown to be especially present in the smallest capillary blood vessels, making their study of particular importance [14-17].

In OPS imaging, the tissue embedding the microcirculation is illuminated with polarized green light [4,19-21]. Backscattered (and thus depolarized) light is projected onto a CCD camera after it passes an analyzer, i.e., a polarizer orthogonally-oriented with respect to the incident polarization. The light reflected by the tissue surface, which is undepolarized, is blocked by this analyzer. By elimination of the reflected light and imaging of only the backscattered light, subsurface structures, such as the microcirculation, can be observed. The use of green light ensures sufficient optical absorption by the (de)oxyhemoglobin-containing red blood cells (RBCs) with respect to the lack of absorption by the tissue embedding the microcirculation, creating contrast (i.e., RBCs are visualized black and tissue is visualized white/grayish).

Despite the major contribution OPS imaging has made in the field of intravital microcirculatory imaging, several shortcomings are still present [19,20,22]. These include suboptimal imaging of the capillaries due to motion-induced image blurring, by movement of the OPS device, the tissue, and/or flowing RBCs. Also in larger vessels, especially during continuous flow, it is difficult to observe the granular nature of flowing blood cells due to blurring of images. This introduces difficulties in measuring blood flow velocities in these vessels.

Driven by the success of OPS imaging and the drawbacks it has, we developed a novel imaging modality for the microcirculation, which we have termed Sidestream Dark Field (SDF) imaging [15,22,23]. In SDF imaging, illumination is provided by surrounding a central light guide by concentrically placed light emitting diodes (LEDs) to provide sidestream dark field illumination (see Fig. 1(a)). The lens system in the core of the light guide is optically isolated from the illuminating outer ring thus preventing the microcirculatory image from contamination by tissue surface reflections. Light from the illuminating outer core of the SDF probe, which penetrates the tissue illuminates the tissue-embedded microcirculation by scattering. The LEDs emit at a central wavelength of 530 nm, chosen to correspond to an isosbestic point in the absorption spectra of deoxy- and oxyhemoglobin (i.e., at λ = 530 nm, $\mu_{a,deoxyHb} = \mu_{a,oxyHb} = 205$ cm^{-1}, [24]) to ensure optimal optical absorption by the hemoglobin in the RBCs, independent of its oxygenation state. This leads to an image where RBCs are imaged as dark moving globules against a white/grayish background). To improve the imaging of moving structures such as flowing RBCs, the LEDs provide pulsed illumination in synchrony with the CCD frame rate to perform intravital stroboscopy. This stroboscopic imaging, (partially) prevents smearing of moving features, such as flowing RBCs, and motion-induced blurring of capillaries due to the short illumination intervals.

In the first part of this study, SDF imaging is validated by comparison of SDF-mediated measurements to OPS-mediated measurements of capillary diameters (CDs) and RBC velocities (RBCVs) in the human nailfold microcirculation. In addition to the validation of SDF imaging, OPS and SDF images of exactly the same microcirculatory areas were obtained sublingually to allow comparison of image quality in the second part of this study. For this purpose, an image quality quantification system was developed to allow quantitative comparison of image quality, in terms of contrast and sharpness, obtained by OPS and SDF images.

#86192 - $15.00 USD Received 7 Aug 2007; revised 11 Oct 2007; accepted 25 Oct 2007; published 31 Oct 2007

2. Materials and methods

2.1 OPS and SDF imaging

For OPS imaging, a Cytocan-II backfocus type device (Cytometrics, Philadelphia, PA) was used [4] and for SDF imaging, a MicroScan Video Microscope (MicroVision Medical, Amsterdam, The Netherlands) was employed. Both the OPS and the SDF devices are fitted with a 5× objective lens system. Illumination intensity was modulated during imaging to obtain visually optimized images for both techniques. To fine-tune the depth of focus of the OPS device, the OPS probe can be axially translated with respect to the fixed CCD camera. In the SDF device, the CCD chip can be axially translated with respect to the fixed lens system in the tip of the SDF probe (see Fig. 1(b)). Covered by a sterile disposable cap, the probes can be placed on organ and tissue surfaces to investigate microcirculatory morphology and perfusion under different clinical conditions. To prevent microcirculatory perfusion alterations by applying pressure on the imaged area, the probes were placed onto the tissue and then gently pulled back until contact was lost [25]. Then the probes were advanced again slowly to the point at which contact was regained and the microcirculation was in focus of the lens systems contained in both probes.

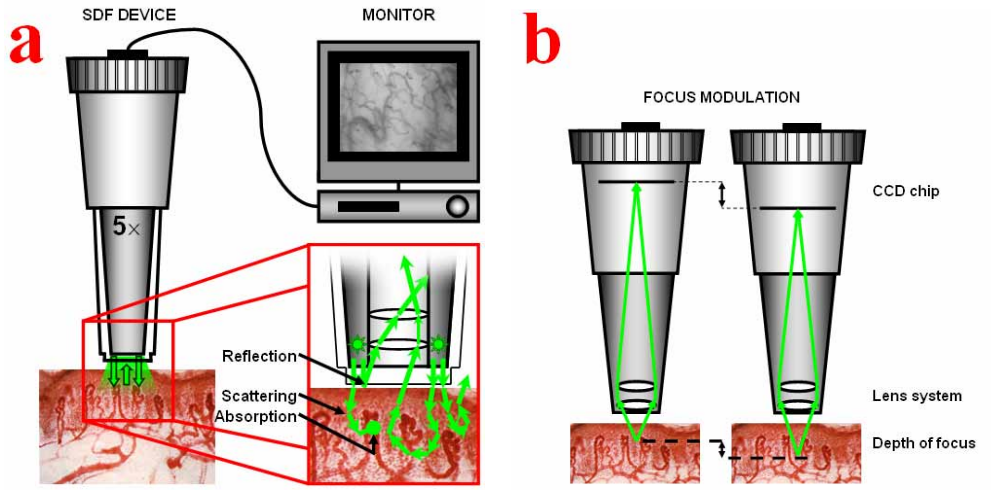

Fig. 1. (a) Left: The hand-held Sidestream Dark Field (SDF) imaging device, equipped with a 5× magnifying objective lens system-containing probe, imaging the tissue-embedded microcirculation using green pulsed LED ring illumination. Upper right corner: Images are recorded using a digital video recorder/computer and visualized on a monitor. Lower right corner: After penetration into the tissue, the illumination light undergoes scattering events (indicated with arrows) and can be absorbed by (de)oxyhemoglobin (indicated with dots). The SDF lens system is optically isolated from the illuminating outer LED ring so that there is no contamination of the microcirculatory images by surface reflections. (b) In the SDF device, the CCD chip can be axially translated with respect to the fixed lens system in the tip of the SDF probe to fine-tune the depth of focus.

Video output was visualized on a monitor and connected to a computer via a signal converter (Canopus, ADVC110) to directly and digitally record images onto a hard drive as DV-AVI files to enable off-line analysis of the images.

The devices were mounted in a specially engineered universal holder (Department of Instrumentation, Academic Medical Center, University of Amsterdam) for accurate positioning and stabilization of both probes and to enable quick and easy interchanging of the devices.

#86192 - $15.00 USD Received 7 Aug 2007; revised 11 Oct 2007; accepted 25 Oct 2007; published 31 Oct 2007

2.2 Subjects

Twenty voluntary potential subjects were screened for a nailfold microcirculation that was clearly visible when applying OPS imaging. Eventually, nine healthy non-smoking male volunteers and one healthy non-smoking female volunteer (mean±SD age was 20±2 year) were selected for this validation study. None of these subjects used any medication and all refrained from drinking coffee at least two hours before the measurements to ensure a stable and uninfluenced nailfold microcirculation.

2.3 Nailfold microcirculatory imaging

Validation of SDF imaging was performed in analogy to our previously published protocol, where OPS imaging was compared to intravital capillaroscopy (i.e., the gold standard for microcirculatory imaging prior to the introduction of OPS imaging) [26]. Briefly, the subjects were seated in a comfortable and stable position with their arms slightly bent at heart level. The fingers of the non-dominating hand were stabilized by pushing them gently into a clay bed. Room temperature was kept between 19 and 22 ^{o}C. By random selection, it was decided which device (OPS or SDF) was to be used first. Paraffin oil was applied to make the highly scattering nailfold skin more translucent. The devices were adjusted for optimal focus and contrast. Images were recorded during rest, venous occlusion, and arterial occlusion to investigate the response of microcirculatory blood vessel diameter and RBC flow to occlusion and release. A cuff, which was inflated in < 5 seconds, was used for venous (cuff pressure = 50 mmHg) and arterial (cuff pressure = 180 mmHg) occlusion. The measurement time table is depicted in Table 1. OPS and SDF images were acquired sequentially during each of the physiological stimuli.

Table 1: Time table of the nailfold microcirculatory imaging protocol.

Measurement		**Cuff**	**Duration**
1.	**Rest**	Deflated	2 minutes
2.	**Venous occlusion**	Inflated to 50 mmHg	2 minutes
	Normalization of microcirculatory perfusion	Deflated	2 minutes
3.	**Arterial occlusion**	Inflated to 180 mmHg	2 minutes

2.4 Skin temperature measurements

To monitor skin temperature during microcirculatory imaging, a thermocouple connected to a digital thermometer (Keithley 871A, Keithley Instruments) was taped proximal to the nailfold onto the skin. In order to avoid temperature influences on the microcirculation (e.g., microcirculatory hypo- or hyperperfusion [26,27]), measurements were excluded from further off-line analysis if skin temperature changed > 1.5 ^{o}C during an imaging period.

2.5 Nailfold microcirculatory measurements

From the nailfold microcirculation, four capillaries were arbitrarily selected for further off-line analysis (see Fig. 2). After stabilization (to eliminate movement artifacts) of isolated video sequences, dedicated software developed was used to analyze microcirculatory blood vessel diameters and RBC kinetics (Microcirculatory Analysis Software (MAS 2.0) Academic Medical Center, University of Amsterdam).

#86192 - $15.00 USD Received 7 Aug 2007; revised 11 Oct 2007; accepted 25 Oct 2007; published 31 Oct 2007

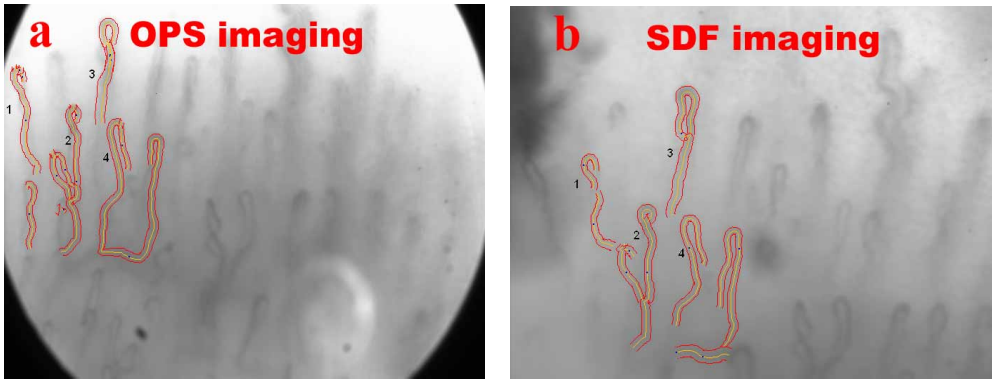

Fig. 2. (a) OPS and (b) SDF image of the same nailfold capillary bed. Four capillaries were selected for further off-line analysis of capillary diameters and red blood cell velocities.

2.6 Sublingual microcirculatory imaging

To compare image quality for OPS and SDF imaging, sublingual images were obtained in two humans. Both subjects were trained in OPS and SDF imaging and were able to locate the same sublingual microcirculatory areas on command. To ease location of the sublingual microcirculatory areas, OPS video frames were saved and printed to serve as guides. During the sublingual recordings, images were optimized by illumination and focus modulation. No off-line image enhancement was performed for both image analysis and publication.

2.7 Sublingual microcirculatory image contrast analysis

After recording the sublingual microcirculation by OPS and SDF imaging, three microcirculatory areas were selected for image quality analysis. In these three areas, one video frame was isolated for both OPS and SDF. Since the functional information in microcirculatory images lies in the capillaries and the venules (i.e., since arterial RBC velocities are typically too high to measure), image quality was determined for each of these vessel types. Therefore, in each of the sublingual microcirculatory video frames, six capillaries and five venules were chosen to perform capillary and venular quality analysis. To quantify capillary and venular quality, we developed a quantification system, which expressed capillary and venular contrast, sharpness, and quality in Image Quality Parameters (IQPs), which scale from 0 (i.e., no contrast) to 1 (i.e., optimal contrast and sharpness).

To determine capillary contrast with respect to the surrounding tissue, cross-sectional grayscale histograms (grayscale value 0 corresponds to black and 255 corresponds to white) were obtained using ImageJ (developed at the US National Institutes of Health, www.nih.gov). The lowest gray value in the capillaries (I_{min}) and the highest gray value in the tissue left ($I_{max,left}$) and right ($I_{max,right}$) of the capillaries were measured. To scale capillary contrast c_{cap} between 0 and 1, c_{cap} was defined as:

$$c_{cap} = \frac{1}{255} \cdot \left(I_{\max} - I_{\min} \right), \text{ where } I_{\max} = \frac{1}{2} \cdot \left(I_{\max,left} + I_{\max,right} \right).$$

For capillary sharpness, the spatial separation in the images between I_{min} and $I_{max,left}$ and $I_{max,right}$ were measured to calculate the maximum slope angles α_{left} and α_{right} of the slopes of the gray value increase at the capillary-tissue interfaces. To scale capillary sharpness s_{cap} between 0 and 1, s_{cap} was defined as:

#86192 - $15.00 USD Received 7 Aug 2007; revised 11 Oct 2007; accepted 25 Oct 2007; published 31 Oct 2007

$$s_{cap} = \frac{1}{90} \cdot \alpha \text{, where } \alpha = \frac{1}{2} \cdot \left(\left| \alpha_{left} \right| + \left| \alpha_{right} \right| \right).$$

For venular quality calculation, cross-sectional grayscale histograms of five venule-tissue interfaces were plotted. In analogy to capillary contrast and sharpness determination, venular contrast and sharpness were also defined using I_{max}, I_{min}, and α:

$$c_{ven} = \frac{1}{255} \cdot \left(I_{\max} - I_{\min} \right) \text{ and } s_{ven} = \frac{1}{90} \cdot \alpha .$$

Ultimately, to scale capillary and venular quality, q_{cap} and q_{ven}, from 0 to 1, q_{cap} and q_{ven} were defined as:

$$q_{cap} = c_{cap} \cdot s_{cap} \text{ and } q_{ven} = c_{ven} \cdot s_{ven} \text{, respectively.}$$

2.8 Statistical analysis

Statistical analysis was performed using Microsoft Excel for means, standard deviations, and Student's t-tests ($p < 0.05$ was considered statistical significantly different) and MedCalc (MedCalc Software, Mariakerke, Belgium) for Bland-Altman distributions [26,28,29].

3. Results

3.1 Scaling factor

In Fig. 3, all CDs measured using SDF are plotted against all measured diameters using OPS to reveal a potential magnification difference between the two devices.

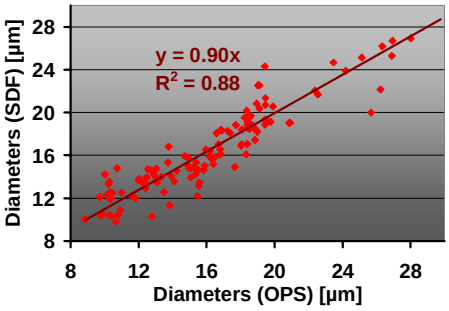

Fig. 3. The capillary and venular diameters measured with SDF plotted against the capillary and venular diameters measured using OPS.

The regression line (slope = 0.90, $R^2 = 0.88$) shows that the CDs measured using the two devices are linearly related, however, a magnification difference exists. The magnification ratio OPS:SDF equals 0.9:1.0, corresponding to on-screen magnifications of 340× and 380× for OPS and SDF imaging, respectively.

During further analysis, the scaling factor ×0.9 is applied for the SDF-mediated measurements to correct for the magnification difference and to allow comparison of CDs and RBCVs for OPS and SDF imaging.

#86192 - $15.00 USD Received 7 Aug 2007; revised 11 Oct 2007; accepted 25 Oct 2007; published 31 Oct 2007

3.2 Nailfold capillary diameters

The measured nailfold CDs are scaled to correct for the magnification difference between the OPS and SDF imaging device. The CDs measured using SDF imaging are shown to be not significantly different (i.e., $p \geq 0.05$) to the measurements performed using OPS imaging, during rest, venous occlusion, and arterial occlusion (see Table 2).

Table 2: Capillary and venular diameters measured with OPS and SDF imaging.

Measurement	**OPS / SDF**	**Mean diameter [µm]**	**Diameter SD [µm]**	**Statistical Significance**
Rest	OPS	15.8	4.9	p = 0.23
	SDF	14.5	4.2	
Venous occlusion	OPS	17.4	4.6	p = 0.25
	SDF	16.2	4.1	
Arterial occlusion	OPS	16.1	4.7	p = 0.08
	SDF	14.4	3.8	

In addition to the Student's t-test, a Bland-Altman distribution is plotted of the measured CDs, where the difference in measured diameter is given as a function of the average diameter measured using OPS and SDF (see Fig. 4). The plot shows an equal distribution of the measurement differences for all averaged diameters.

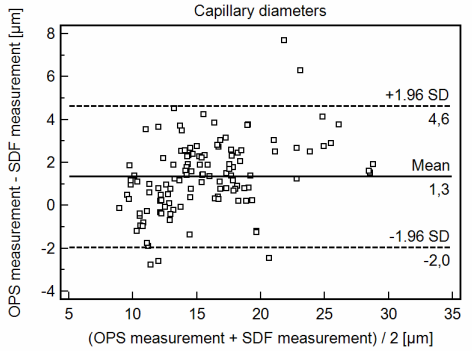

Fig. 4. The Bland-Altman plot depicting the measured diameter difference between the techniques as function of the average measured diameter. SDF measurements are corrected, applying a scaling factor, to allow comparison of diameters measured using OPS and SDF.

3.3 Nailfold capillary red blood cell velocities

Using MAS 2.0, OPS imaging allowed the measurement of RBCVs by the use of space-time diagrams [30] in 36 out of the 40 capillaries, while SDF imaging allowed these measurements in 39 out the 40 capillaries. The capillaries in which the RBCV could not be determined were hyperperfused resulting in velocities beyond the detection of the frame rate of the CCD camera (i.e., > 750 pixels/sec) [31].

Table 3: Capillary and venular red blood cell velocities measured with OPS and SDF imaging.

Measurement	**OPS / SDF**	**Mean velocity [µm/sec]**	**Velocity SD [µm/sec]**	**Statistical Significance**
Rest	OPS	277.2	93.7	p = 0.11
	SDF	243.1	86.7	
Venous occlusion	OPS	83.3	37.4	p = 0.67
	SDF	79.9	33.8	
Arterial occlusion	OPS	0.0	0.0	p = 1.00
	SDF	0.0	0.0	

#86192 - $15.00 USD Received 7 Aug 2007; revised 11 Oct 2007; accepted 25 Oct 2007; published 31 Oct 2007

The measured nailfold capillary RBCVs are scaled to correct for the magnification difference between the OPS and SDF imaging device. Nailfold capillary RBCV measurements revealed no significant differences between OPS and SDF imaging during rest, venous, and arterial occlusion (see Table 3). This is also reflected in the Bland-Altman plots in Fig. 5, which show that the measurements differences are equally distributed across the range of measured values and there are no significant systematic differences.

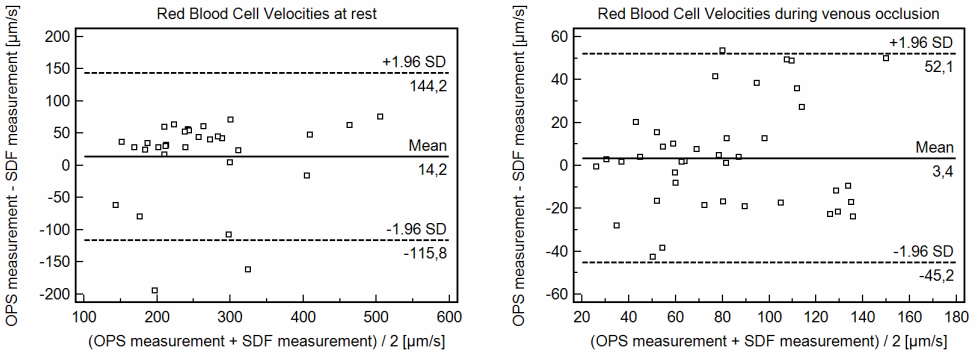

Fig. 5. Two Bland-Altman plots for red blood cell velocity measurements during rest (left) and during venous occlusion (right).

Microcirculatory perfusion completely stopped during arterial occlusion as observed by both OPS as SDF imaging. The RBCVs during venous occlusion were significantly lower than during rest for both OPS ($p < 0.0001$, not shown in table) and SDF imaging ($p < 0.0001$, not shown in table).

3.4 Sublingual microcirculatory image quality

SDF image quality is compared to OPS image quality of sublingually-obtained microcirculatory areas and is expressed in IQPs as outlined in the Materials and Methods section. To allow comparison of capillary and venular sharpness obtained using OPS and SDF imaging, where spatial separation in the images between I_{max} and I_{min} are used in the calculations, SDF measurements are corrected for the magnification difference between the OPS and the SDF device.

SDF imaging provided superior image quality, divided in capillary quality and venular quality, with respect to OPS imaging as is depicted in Table 4. Capillary quality is shown to be significantly higher for SDF imaging compared to OPS imaging ($p = 0.02$), originating solely from higher contrast (i.e., 0.06±0.03 for OPS imaging and 0.09±0.05 for SDF imaging), since capillary sharpness was equal for both techniques (i.e., 0.86±0.08 for OPS imaging and 0.88±0.06 for SDF imaging). Venular quality is shown to be equal for OPS and SDF imaging ($p = 0.57$).

Table 4: Capillary and venular contrast, sharpness, and quality of sublingually-obtained microcirculatory images.

	Modality	**Contrast**	**Sharpness**	**Quality**	
Capillaries	OPS	0.06±0.03	0.86±0.08	0.05±0.03	p = 0.02
	SDF	0.09±0.05	0.88±0.06	0.08±0.05	
Venules	OPS	0.19±0.09	0.82±0.09	0.16±0.08	p = 0.57
	SDF	0.22±0.10	0.81±0.08	0.18±0.08	

In Fig. 6(a) and 6(b), the capillary and venular quality for OPS and SDF imaging are illustrated. Figure 6(a) clearly shows that capillaries have higher contrast using SDF than using OPS imaging. Venular contrast and sharpness is approximately equal for both

#86192 - $15.00 USD Received 7 Aug 2007; revised 11 Oct 2007; accepted 25 Oct 2007; published 31 Oct 2007

techniques as shown in Fig. 6(b). Additionally, the figures depict the magnification difference between the OPS and SDF device (see scale bars Fig. 6(a) and 6(b)).

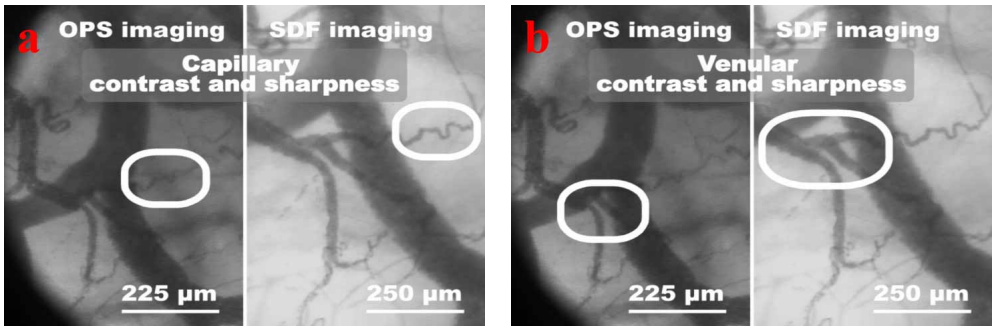

Fig. 6. (3.2 MB) Movie: OPS imaging versus SDF imaging of the sublingual microcirculation (12.6 MB version). (a) Capillary contrast and sharpness. (b) Venular contrast and sharpness. The scale bars indicate the magnification difference between the OPS and SDF device.

In Fig. 7(a) and 7(b), individual RBCs can be observed using SDF imaging. The capillary loop, indicated with an arrow in Fig. 7(a), is perfused with individual RBCs (numbered from 1 to 7) and plasma gaps as is shown in Fig. 7(b).

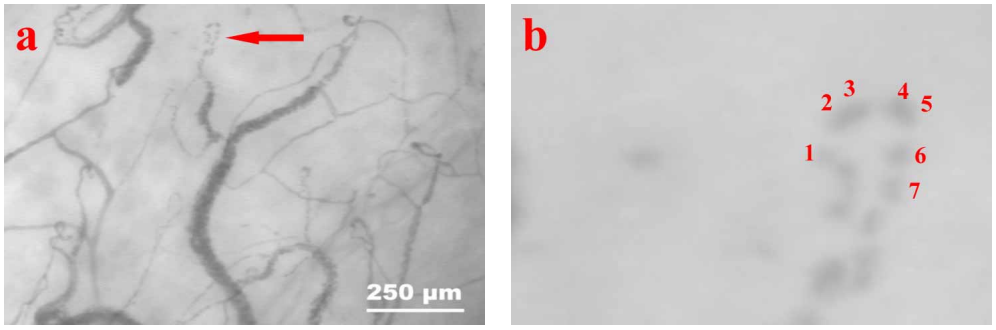

Fig. 7. (1.8 MB) Movie: SDF imaging of a capillary loop (13.8 MB version). Individual red blood cells (numbered from 1 to 7 in the (b) panel) and plasma gaps flowing through a capillary can be observed in normal view (a) and in the zoomed view (b).

4. Discussion

This study introduced a novel optical technique for clinical observation and assessment of the microcirculation, termed Sidestream Dark Field (SDF) imaging, and validated it by comparing it to OPS imaging. Results showed that OPS and SDF imaging provided similar quantitative values for CDs and RBCVs in the human nailfold microcirculation and that SDF imaging provides improved image quality with respect to OPS imaging as shown in sublingual microcirculatory recordings. These basic findings validate the use of SDF imaging for clinical measurement of microcirculatory vessel diameters and RBCV measurements.

To allow quantitative comparison of image quality obtained using OPS and SDF imaging in the second part of this study, an image quality quantification system was developed. This system scaled capillary and venular contrast, sharpness, and quality in OPS and SDF video frames on scales from 0 to 1. The analysis of images of multiple microcirculatory areas, imaged with both OPS and SDF, has shown that SDF imaging provides significantly better capillary contrast and quality and equal venular contrast, sharpness, and quality with respect to OPS imaging (see Fig. 6).

#86192 - $15.00 USD Received 7 Aug 2007; revised 11 Oct 2007; accepted 25 Oct 2007; published 31 Oct 2007

SDF images also showed increased resolvability of the granular nature of flowing RBC columns in venules, compared to OPS images. This latter is an important improvement, because software-mediated analysis of RBCVs is based on the detection of moving structures and determination of their velocities [26,30,31]. This is exemplified in the movie of Fig. 8, where the pulsatile flow can be readily followed due to the high granularity of the venular RBC column.

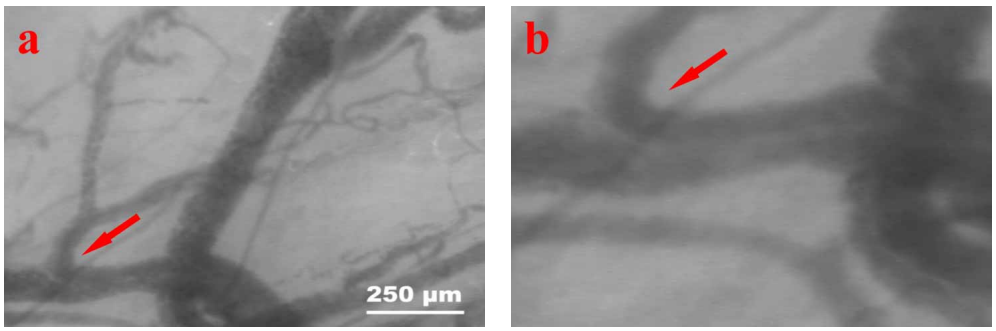

Fig. 8. (3.0 MB) Movie: Pulsatile flow as observed using SDF imaging. (12.1 MB version). Note the high granularity of the red blood cell column in the venules. The arrows indicate the venular junction where pulsatile flow is observed. Panel (b) is an enlarged view of the pulsatile part in panel (a).

SDF imaging can image individual RBCs and plasma gaps flowing through capillaries clearly as depicted in Fig. 7. In addition, leukocytes could be observed using the SDF device (see Fig. 9). Leukocyte rolling can be observed using both OPS and SDF imaging [32]. In Fig. 9(b), most leukocytes travel from the vertical capillary via the T-junction to the right capillary. As the capillary increases in diameter, the leukocytes start rolling till they reach the capillary-venule junction. Once arrived in the venule some leukocytes remain rolling against the venular wall and others are taken up by the blood flow and slowly flow down-stream.

Increased microvascular quality and observability of granular structures probably originates from the stroboscopic illumination, which prevents smearing of moving features such as RBC columns in capillaries and venules. Stroboscopic imaging also reduces image blurring due to movement of the device and/or the tissue. An additional contributing factor to the superior quality of SDF imaging is the shallower focusing depth of the SDF device with respect to the focus of the OPS device. In OPS imaging, underlying vascular (and thus light absorbing) structures (partially) darken the image, lowering image contrast and quality (see Fig. 6). In SDF imaging however, these underlying structures do not interfere, due to the shallow imaging depth of the SDF device, and therefore provide clear images of the superficial microcirculatory network.

In addition to the superior image quality, SDF imaging has the advantage of low-power LED illumination, which allows battery and/or (portable) computer operation and thereby improved clinical applicability. For OPS imaging, relatively strong light sources and thus mains power supply are required, since a large portion of the illumination light is blocked by the first polarizer and another substantial amount of light is reflected by the tissue surface, which do not contribute to the image formation. These high power light sources limit the portability and clinical applicability of OPS imaging. Since SDF employs low-power LEDs for illumination, no isolation transformers between the device and mains power supply are required to protect current leakage in operating rooms, intensive care units, and emergency rooms. Furthermore, battery operation allows microcirculatory measurements recordings to be made in conditions such as ambulances, and emergency and combat medicine, where mains power is not always available.

#86192 - $15.00 USD Received 7 Aug 2007; revised 11 Oct 2007; accepted 25 Oct 2007; published 31 Oct 2007

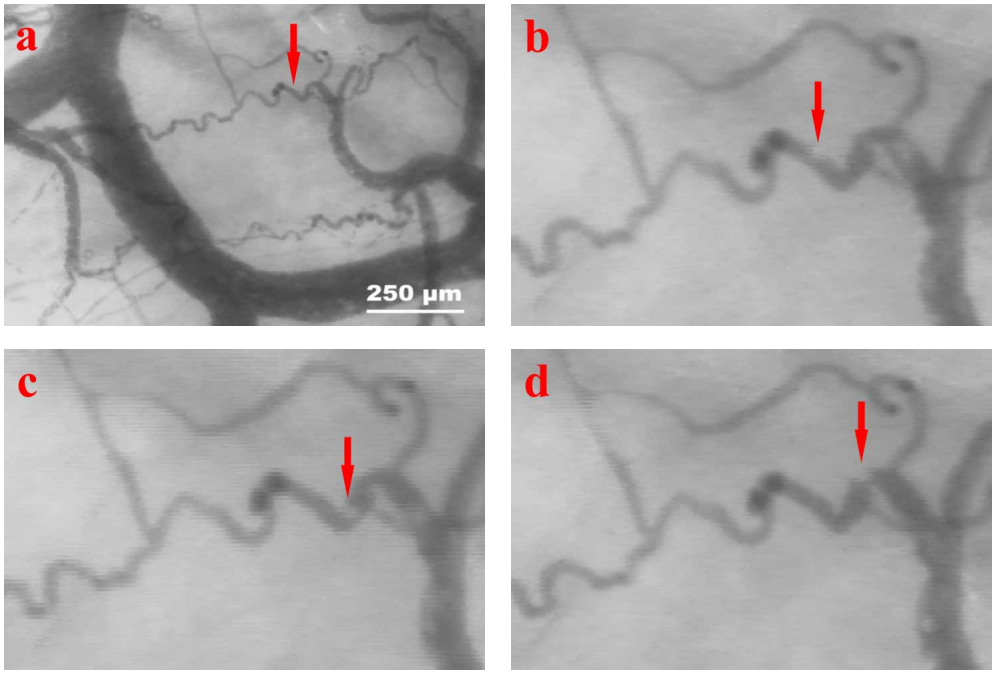

Fig. 9. (4.0 MB) Movie: Leukocyte visualization using SDF imaging (14.1 MB version). SDF imaging enables leukocyte visualization: (a) normal view, (b,c, and d) zoomed view. The red arrows indicate a rolling leukocyte at (a,b) t = 0 ms, (c) t = 400 ms, and (d) t = 800 ms.

Increased microvascular quality and observability of granular structures probably originates from the stroboscopic illumination, which prevents smearing of moving features such as RBC columns in capillaries and venules. Stroboscopic imaging also reduces image blurring due to movement of the device and/or the tissue. An additional contributing factor to the superior quality of SDF imaging is the shallower focusing depth of the SDF device with respect to the focus of the OPS device. In OPS imaging, underlying vascular (and thus light absorbing) structures (partially) darken the image, lowering image contrast and quality (see Fig. 6). In SDF imaging however, these underlying structures do not interfere, due to the shallow imaging depth of the SDF device, and therefore provide clear images of the superficial microcirculatory network.

In addition to the superior image quality, SDF imaging has the advantage of low-power LED illumination, which allows battery and/or (portable) computer operation and thereby improved clinical applicability. For OPS imaging, relatively strong light sources and thus mains power supply are required, since a large portion of the illumination light is blocked by the first polarizer and another substantial amount of light is reflected by the tissue surface, which do not contribute to the image formation. These high power light sources limit the portability and clinical applicability of OPS imaging. Since SDF employs low-power LEDs for illumination, no isolation transformers between the device and mains power supply are required to protect current leakage in operation rooms, intensive care units, and emergency rooms. Furthermore, battery operation allows microcirculatory measurements recordings to be made in conditions such as ambulances, and emergency and combat medicine, where mains power is not always available.

However, although SDF imaging was shown to be superior to OPS imaging, it still suffers from some shortcomings. In the current SDF device, the detectable RBCV is physically limited (at approximately 1 mm/s) by the length of the observed vessels in combination with the 25 fps (PAL) or 30 fps (NTSC) acquisition rates. Thus, future improvement of SDF

#86192 - $15.00 USD Received 7 Aug 2007; revised 11 Oct 2007; accepted 25 Oct 2007; published 31 Oct 2007

imaging will be made by incorporation of more advanced camera technology in terms of resolution and frame rate.

A further point of concern with SDF imaging is the pressure-induced microcirculatory alterations by application of the SDF probe onto organ and tissue surfaces. These pressure-induced effects occur with other surface flow/perfusion measurements, such as OPS imaging and laser Doppler velocimetry, as well and might lead to false interpretation of the actual microcirculatory perfusion (see Fig. 10). To prevent the microcirculatory measurements from this pressure artifact during OPS imaging, Lindert et al. engineered an extending click-on ring, which was placed around the OPS probe. By applying suction via holes in the ring using a vacuum pump, the tissue in the center, that was imaged through the OPS probe, was inhibited from moving and the pressure on the imaged vasculature was reduced [19,25]. However, when applied sublingually, complications occurred due to suction of salvia underneath the OPS probe, creating image-disturbing bubbles. Hence, an elegant solution, which provides pressure-reduction, fluid-extraction, and motion-inhibition, still remains to be developed.

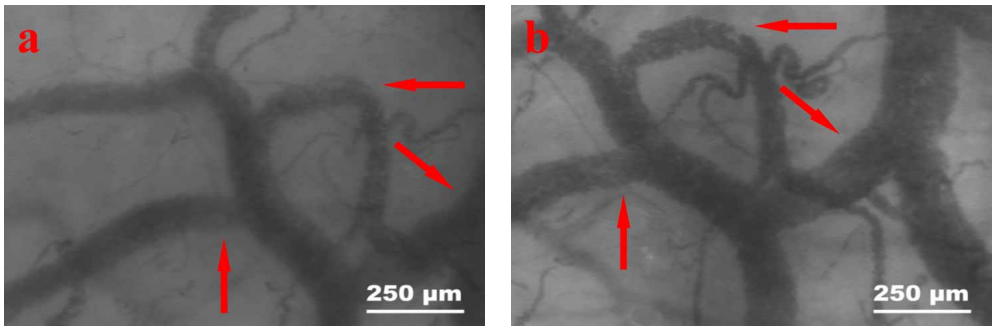

Fig. 10. (3.1 MB) Movie: Pressure artifact during SDF imaging (9.8 MB version). (a) No application of pressure. (b) Application of pressure. Observability of venular granularity depends of blood flow velocity as can be seen at the sites indicated with arrows.

5. Conclusions

In conclusion, the present study has introduced a novel imaging modality, which can be incorporated into a hand-held clinically-applicable device, called Sidestream Dark Field imaging. SDF imaging was validated by quantitative comparison to OPS imaging. Additionally, this study introduced an image quality quantification system, which has shown the capability of quantifying image quality differences in a statistical significant manner.

SDF and OPS images provided similar quantitative data in terms of vessel diameters and RBCVs. SDF imaging, moreover, provided significantly higher image quality with more detail, capillary contrast and quality, granularity of venular RBC columns, and less motion blur by the use of stroboscopic LED ring-based sidestream dark field illumination.

It is anticipated that SDF imaging will serve as a novel and improved imaging modality to contribute to the clinical assessment of the microcirculation in various clinical scenarios and, additionally, allow more reliable application of computer-aided image processing and analysis software for quantification of microcirculatory alterations associated with disease and therapy.

Declared interests and acknowledgements

Can Ince is, besides his position in the Academic Medical Center (AMC), chief scientific officer of an AMC spin-off company, called MicroVision Medical, which has commercialized SDF imaging into a device termed the Microscan.

#86192 - $15.00 USD Received 7 Aug 2007; revised 11 Oct 2007; accepted 25 Oct 2007; published 31 Oct 2007

The authors thank Dan M. J. Milstein for making the recordings of his sublingual microcirculation for this study.

This work was supported by the Landsteiner Foundation for Blood Transfusion Research (Grand No: 0621).

#86192 - $15.00 USD Received 7 Aug 2007; revised 11 Oct 2007; accepted 25 Oct 2007; published 31 Oct 2007